Power Flow for Resonance Cone Phenomena in Planar Anisotropic Metamaterials

Keith G. Balmain, *Life Fellow, IEEE*, Andrea A. E. Lüttgen, *Associate Member, IEEE*, and Peter C. Kremer

***Abstract*—The metamaterial considered is a planar wire-grid network loaded with closely spaced, orthogonal capacitors and inductors, positioned over a ground plane and parallel to it. Excited by a single-frequency point source, this metamaterial exhibits conical high-field regions called "resonance cones" which extend outward from the source in directions predetermined by the load reactances, thus carrying RF power to specific points on the resistively terminated network edges. When two such metamaterials are interfaced, the cones traversing the interface can exhibit negative refraction as well as subwavelength focusing, phenomena supported by physical experiments and corresponding moment-method simulations. Poynting vector calculations based on the simulation data reveal power flow that follows the cones smoothly from the source and across the refraction interface. Electromagnetic field and Poynting vector calculations both exhibit potentially significant differences depending on whether they are done at the ground plane level or at the level of the anisotropic grid.**

***Index Terms*—Anisotropic metamaterial, backward refraction, negative refractive index, planar metamaterial, resonance cone power flow, subwavelength focusing.**

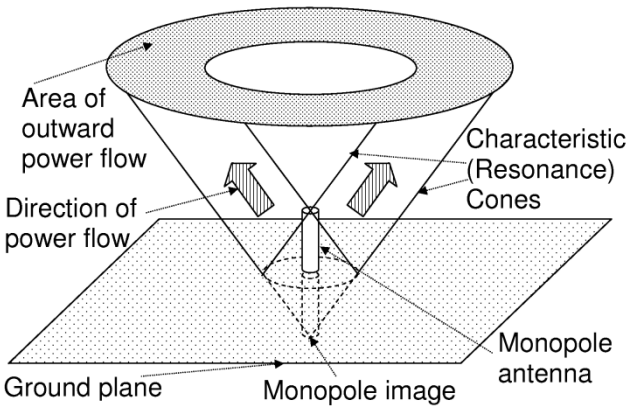

Fig. 1. Monopole antenna in highly anisotropic (resonant) plasma, showing characteristic cones (resonance cones) extending from antenna ends, along with the directions of power flow.

I. Introduction

THE present paper has its roots in two fields of research, namely antennas in anisotropic plasmas and microstructured "metamaterials." In the case of antennas in anisotropic (magnetized) plasmas, resonance cones are conical high-field regions that extend outward from antennas under (lossless) conditions such that two of the three diagonal elements of the plasma permittivity matrix have opposite signs. Early analytical works were those of Bunkin [1], Kogelnik [2], and Kuehl [3]. Fisher and Gould [4] were first to measure the high-field regions, and also apparently first to call them "resonance cones." A recent paper by James [5] on antennas and resonance cones in the ionospheric plasma serves as both a contribution and an up-to-date review of the subject matter.

In mathematical terms, the vacuum wave equation in space-time is a hyperbolic partial differential equation whose characteristic surface (along which discontinuities propagate) is in the shape of a cone. Surprisingly, for anisotropic plasmas excited at a single frequency, it was pointed out by Balmain [6] that the time-reduced quasi-static partial differential equation for the scalar potential can also be hyperbolic, but in the space coordinates alone, showing that the associated conical characteristic surfaces are just the resonance cones already mentioned. In the same paper, Balmain associated an outward power flux with the region between the particular near-field resonance cones that extend from the antenna extremities, as depicted in Fig. 1. Later, Balmain and Oksiutik [7] noted that the plasma negative and positive permittivities could be interpreted by representing the medium in terms of arrays of inductors and capacitors respectively, and that interchanging the inductors and capacitors corresponds to moving the operating point from one hyperbolic region to the other in the parameter space shown in Fig. 2 and known as the CMA diagram (recognizing the contributions of Clemmow, Mullaly, and Allis, as described for example by Yeh and Liu [8]). Further on in the present paper, it will be shown how these two hyperbolic regions serve to suggest two quite different periodic physical media that, when interfaced, display unusual refraction phenomena.

If we choose to regard the inductors and capacitors as physical entities and not just as aids to interpretation, a physical inductor-capacitor (L-C) network becomes an artificial material or "metamaterial" that could exhibit resonance cone phenomena. Moreover, if the L-C network is a planar, square-celled wire grid series-loaded with orthogonal inductors and capacitors and located over a ground plane as shown in Fig. 3, then this structure emerges as a finite-size, two-dimensional (2-D) resonance-cone metamaterial that is straightforward to construct and readily accessible to a variety of electrical testing techniques. If we adopt temporarily the somewhat oversimplified viewpoint of circuit theory, we can see that the resonance cone directions are just

Manuscript received October 2, 2002; revised January 24, 2003. This work was supported by the Natural Sciences and Engineering Research Council of Canada.

The authors are with The Edward S. Rogers Sr. Department of Electrical and Computer Engineering, University of Toronto, Toronto, ON M5S 3G4, Canada (e-mail: balmain@waves.utoronto.ca).

Digital Object Identifier 10.1109/TAP.2003.817542

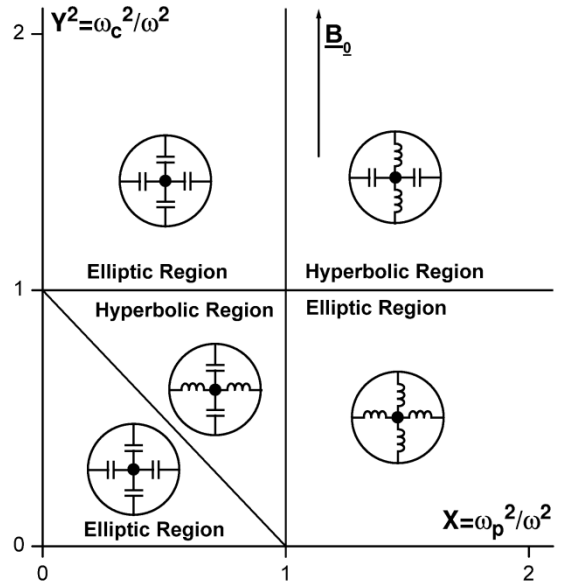

Fig. 2. Plasma parameter diagram showing the elliptic and hyperbolic regions that characterize the relevant partial differential equation. The vertical axis involves the electron cyclotron frequency ω_c and is proportional to the square of the ambient magnetic field, while the horizontal axis involves the plasma frequency ω_p and is proportional to the ambient electron density. The capacitor and inductor symbols characterize the impedance properties of the plasma medium as they affect the input impedance of a small, spherical RF probe immersed in the plasma.

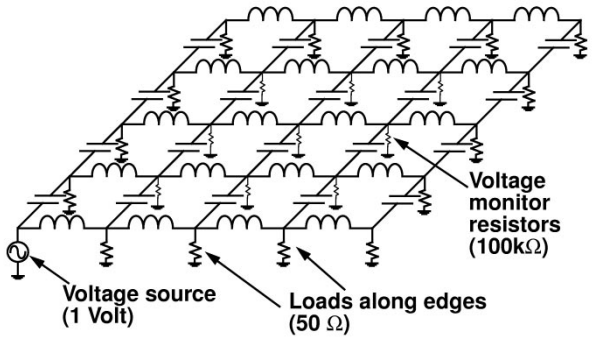

Fig. 3. Uniform anisotropic planar *L-C* grid over ground, with corner feed and resistive edge-loading. The voltage monitor resistors are employed only in the computer simulation.

the directions of the point-to-point zeros in reactance measured across the grid surface.

The current research interest in metamaterials grew from the pioneering theory of Veselago [9] on effectively isotropic "left-handed" materials (having at the same time both negative permittivity and negative permeability), which led to the recent work of Pendry [10] directed toward using these materials to make a "perfect" lens. Such a lens requires negative refraction and enables point-source focusing, properties which in metamaterials take place through a single planar interface between left- and right-handed media or through a planar layer of left-handed material. It should be kept in mind that the "point-source focusing" mentioned above could imply *point imaging* only under highly idealized conditions. The first clear measurement of the needed negative refraction at a planar interface was carried out at microwave frequencies by the team led by Smith and Schultz at UC San Diego [11] using a volume distribution of cellular composite metamaterial with each physically separate cell made up of a resonant wire plus a resonant loop. The most recent success in this isotropic-material category is the demonstration of both negative refraction and point-source focusing by Eleftheriades *et al.* at the University of Toronto using a thin, planar left-handed material consisting of a backward-wave *L-C* network laid out over a ground plane [12].

II. Results for Highly Anisotropic Media Supporting Resonance Cones

For the representation of anisotropic materials, the simulations employed a full-electromagnetic, thin-wire moment-method program [13] which permits the insertion of lumped circuit elements in finite-length wire segments. The basic network simulated was as shown in Fig. 3, consisting of 12 by 12 cells, each cell 2.5 mm square, for a total grid size of 30 by 30 mm, with the grid 2.5 mm above the ground plane. The capacitance was 2 pF per segment and the inductance 5.6 nH per segment, values chosen for availability as well as to achieve the desired resonance-cone effects using existing *X-Y* scanning and network analysis equipment. The inductors used in the experiment had a manufacturer nominal quality factor Q of around 27. This was achieved in the simulation by adding a 1.6 Ω resistor in series with each inductor. A resistor of the same value was added in series with each capacitor as well. Also shown in Fig. 3 is a 100 kΩ resistor from each grid intersection to ground to enable deduction of the grid-to-ground voltage from the computed resistor current. Along the edges, 50 Ω resistors were connected to ground in place of the 100 kΩ resistors. For this value of edge resistance, resonance cone specular reflection from the edges is not significant. The first, limited-scope results using the indicated apparatus and moment-method computer program were published in a letter by Balmain *et al.* [14], in which cone formation, refraction, and focusing were outlined.

The present paper expands on the previous work in part by the use of Poynting vector calculations, thereby tracking power flow and adding emphasis to the electromagnetic aspects of the phenomena. Contour plots of grid-to-ground voltage magnitude and the Poynting vector real parts evaluated from the electric and magnetic fields on the ground-plane level at the center of each cell for corner feed are shown in Fig. 4 which displays the simulated resonance cones and the way the cone orientation scans with frequency over the eight frequencies employed. From the Poynting vector plot it can be seen that power flow is directed along the resonance cones. Apparent specular reflection from the grid edges is sometimes visible (for example, at 0.7, 0.9, 1.9, and 2.3 GHz) but generally it is weak. As well, very weak parasitic resonance cones can be seen in Fig. 4 (for example at 0.9 and 2.3 GHz), probably caused by scattering from the inhomogeneities inherent in the grid structure. In view of the metamaterial's potential use as an instantaneous, passive spectrum analyzer, Fig. 5 shows the frequency response for the voltages across the 50 Ω resistors to ground at all points along two edges of the grid.

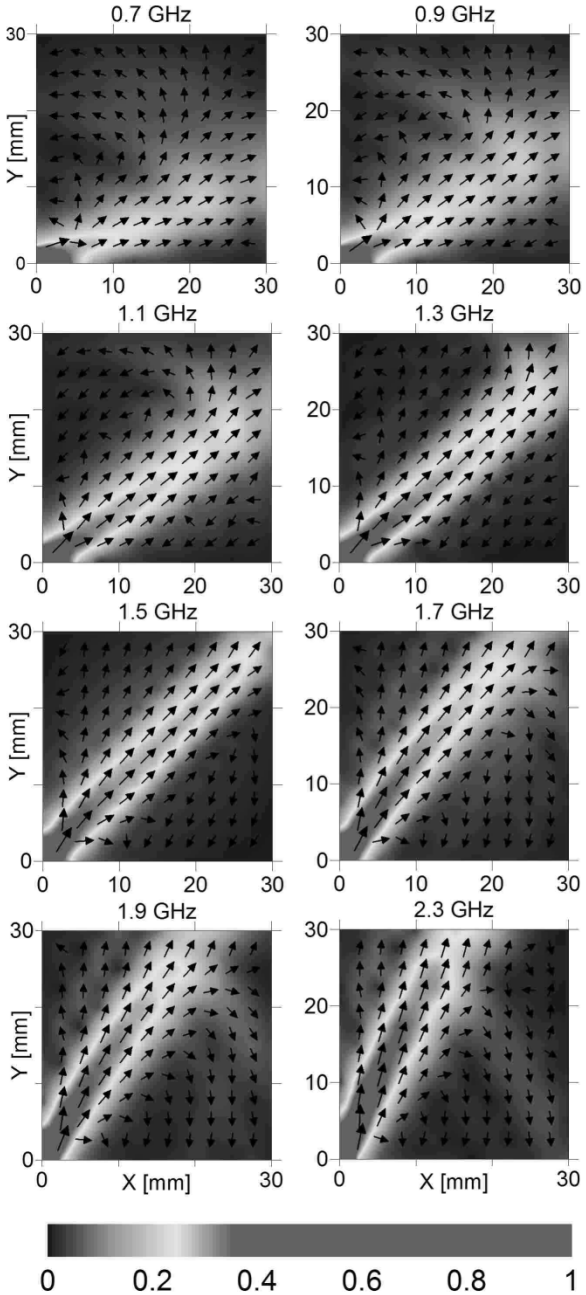

Fig. 4. Uniform-grid moment-method simulation displaying corner-fed resonance cones at eight frequencies. Shown is the grid-to-ground voltage magnitude in volts for a source magnitude of 1 V. The arrows depict the Poynting vector real parts calculated on the ground plane.

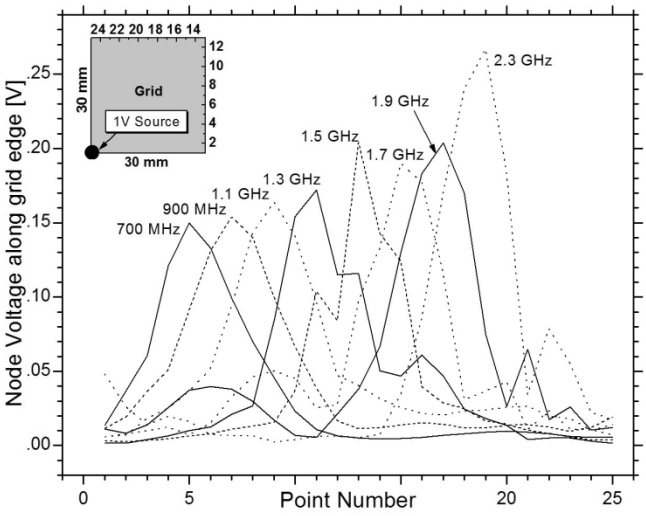

Fig. 5. Node voltage across the 50 Ω terminating resistors at numbered points around the grid edge for the corner-fed configuration of Fig. 3, derived from the simulation data displayed in Fig. 4.

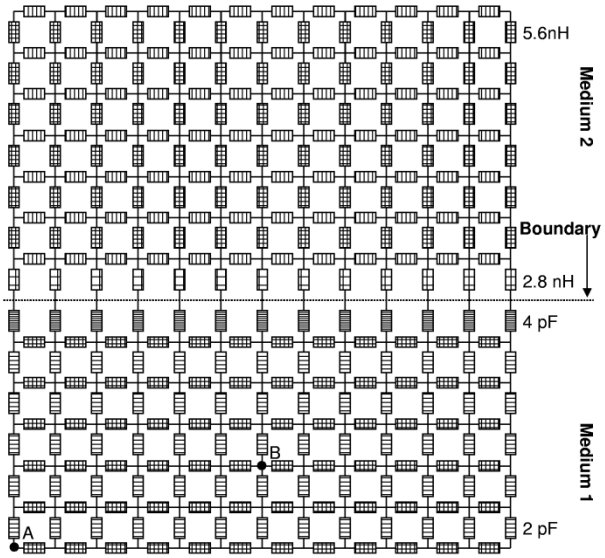

Fig. 6. Schematic view of the nonuniform *L*-*C* grid used in the experiment. Inductors and capacitors have been transposed in the upper part of the grid, relative to the lower part. The transition region consists of a row of elongated cells centered 15 mm from the lower edge. The feed points are at A for refraction measurements and at B for focusing measurements.

To deal with refraction, a different planar medium was created by interchanging (transposing) the inductors and capacitors in the grid in the manner suggested by Fig. 2 and its associated text in Section I of this paper, thus enabling a two-medium configuration with a linear interface between the original medium and the transpose medium. Its component layout is shown in Fig. 6, and its physical realization is shown in Fig. 7 in which the grid elements are chip-type surface-mount inductors and capacitors soldered together. This grid has 12 by 12 cells, where medium 1 (inductors on the horizontal segments, capacitors on the vertical segments) consists of the lower five rows of 12 cells, and medium 2 (capacitors on the horizontal segments, inductors on the vertical segments) consists of the upper six rows of 12

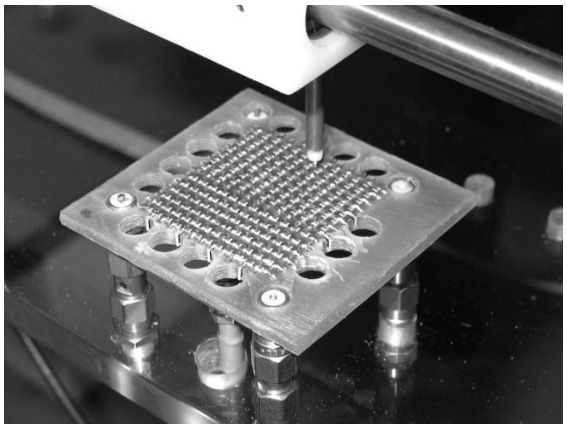

Fig. 7. Experimental setup with scanning open-ended probe.

cells. The sixth row of cells is the transition region where the lower edges of the cell carry inductive loads, the upper edges capacitive loads, and the vertical segments carry a capacitor on the lower half and an inductor on the upper half. Therefore the boundary between the two media lies in the middle of the transition row. To accommodate the physical size of the chip-type inductors and capacitors, the cells in the transition region have to be elongated, i.e., the vertical dimension is doubled compared to cells elsewhere in the grid. The overall size of the setup is 30 by 32.5 mm and the boundary is a horizontal line 15 mm from the bottom of the grid.

In the refraction experiments, the vertical E-field is picked up by an open-ended coaxial probe positioned sequentially just above each conductor intersection, and the probe signal is fed to a network analyzer with output S21 which, when plotted on a linear scale, is approximately proportional to the grid-to-ground voltage. The two-medium result for corner feed (the feed point is below point A in Fig. 6) is shown in Fig. 8 which displays clearly the negative refraction of the resonance cone as it traverses the transposition interface. Notice that specular reflection from the interface is negligible and there is no visible transmission into the second medium in the same direction as the incident cone. This can also be seen from the Poynting vectors in the bottom plot of Fig. 8, which displays the simulation results, where the power flow associated with specular reflection from the interface is negligible and no power along the original resonance cone is transmitted into the second medium.

In order to extend the refraction results to include focusing, the physical setup of Fig. 7 was used with coaxial feed from beneath the ground plane to point B on the grid in Fig. 6, near the middle of one of the two planar metamaterials. At 1.3 GHz, the simulation and experimental results are shown in Figs. 9 and 10, and, at 1.7 GHz, the corresponding results are shown in Figs. 11 and 12. In all cases, one can see the cones emanating from the feed point (the "source"), the backward refraction at the $\mathrm{y} = 15\,\mathrm{mm}$ interface, and the cones merging at the "focus." Note that in Figs. 9 and 11 the power flow closely follows the directions of the resonance cones. Furthermore, Fig. 11 shows the power flow emanating from the source and following the resonance cones to converge at the focus, from where it diverges again into a new set of resonance cones. In Figs. 11 and 12, the focal region is taken to be bounded by the contour that is at 0.707 of the focal region maximum, so this contour may be termed the "half-power" contour. It is worth noting at 1.7 GHz that the experimental focal region boundary lies within a square measuring 1/25th free-space wavelength on a side, so the phenomenon properly may be termed "subwavelength focusing." In contrast, at 1.3 GHz the focal point is too close to the upper edge of the material to exhibit an equally well localized focal region, and thus this represents a useful low-frequency limiting case for the particular overall grid size in use. As well, with increasing frequency, it should be noted that the focal region moves gradually toward the boundary between the two media.

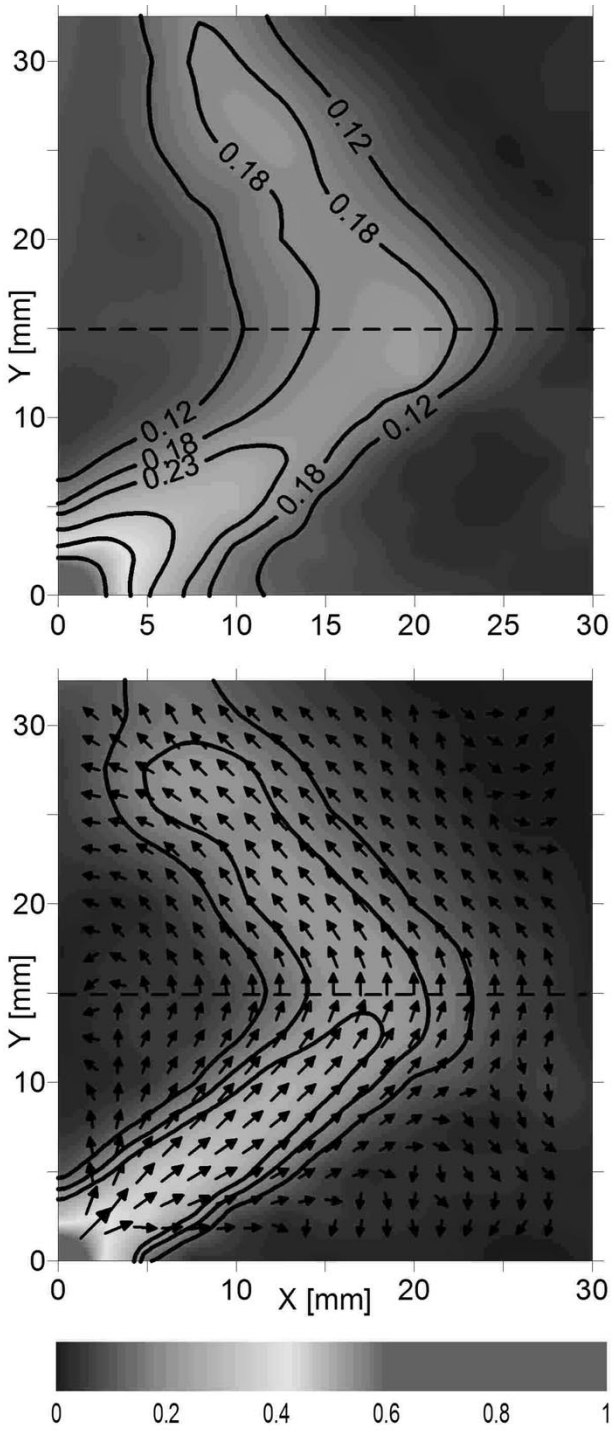

Fig. 8. Resonance-cone refraction at 1.2 GHz — experiment (top) showing contours of normalized $|S21|$, and simulation (bottom) showing contours of grid-to-ground voltage magnitude with arrows depicting the Poynting vector real parts calculated on the ground plane. The contour lines in the bottom plot are at the same levels as the three lowest contour lines in the top plot.

III. Electromagnetic Fields and Power Flow Distribution

Simulation results presented in the previous section made use of the node voltages because they are approximately proportional to the measured S21 values taken immediately above the nodes, thus making experiment and simulation comparable. In this section we take a closer look at the simulated electric and magnetic fields on the grid plane and on the ground plane, because they cannot easily be determined experimentally, and then we use these fields to compute the Poynting vector in the two planes.

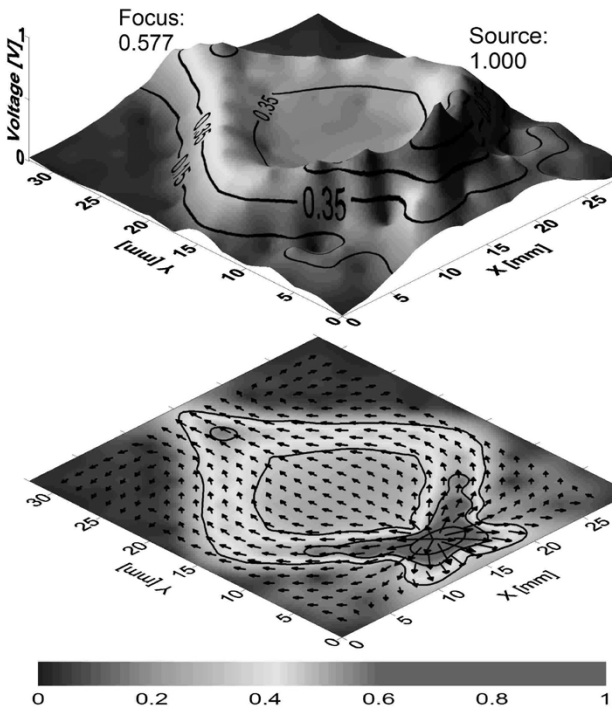

Fig. 9. Focusing simulation at 1.3 GHz showing the grid-to-ground voltage magnitude. The arrows display the Poynting vector real parts calculated on the ground plane.

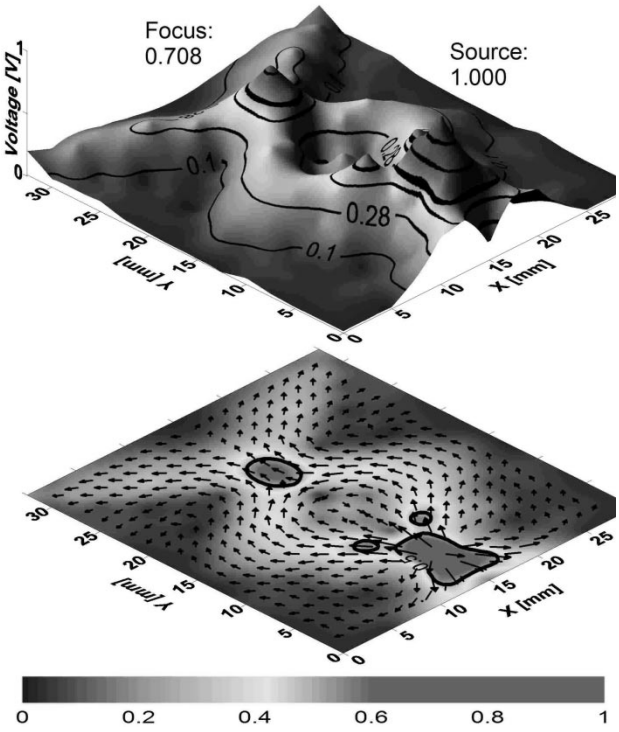

Fig. 11. Focusing simulation at 1.7 GHz showing the grid-to-ground voltage magnitude. Heavy contour is at 0.707 of focal maximum of 0.708 V magnitude. The arrows display the Poynting vector real parts calculated on the ground plane.

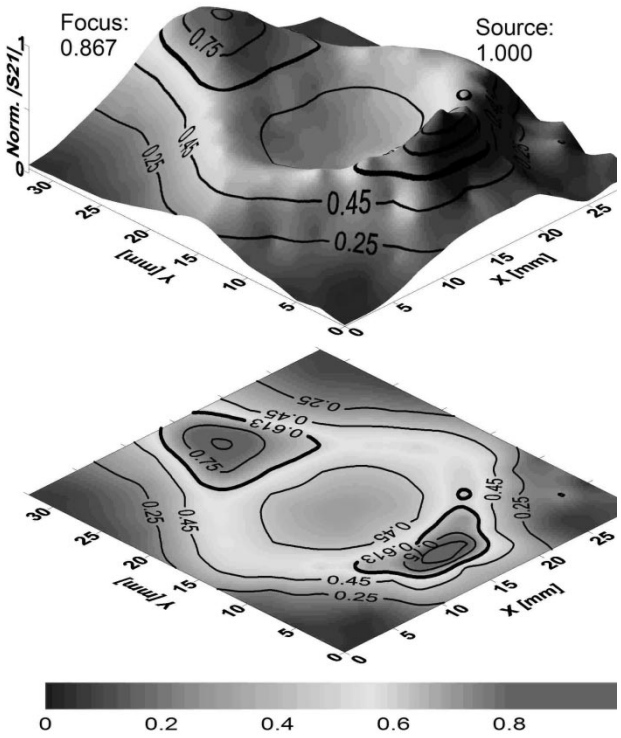

Fig. 10. Focusing measurements at 1.3 GHz showing the normalized S21 magnitude. Heavy contour is at 0.707 of focal maximum of 0.867 (units of normalized $|S21|$).

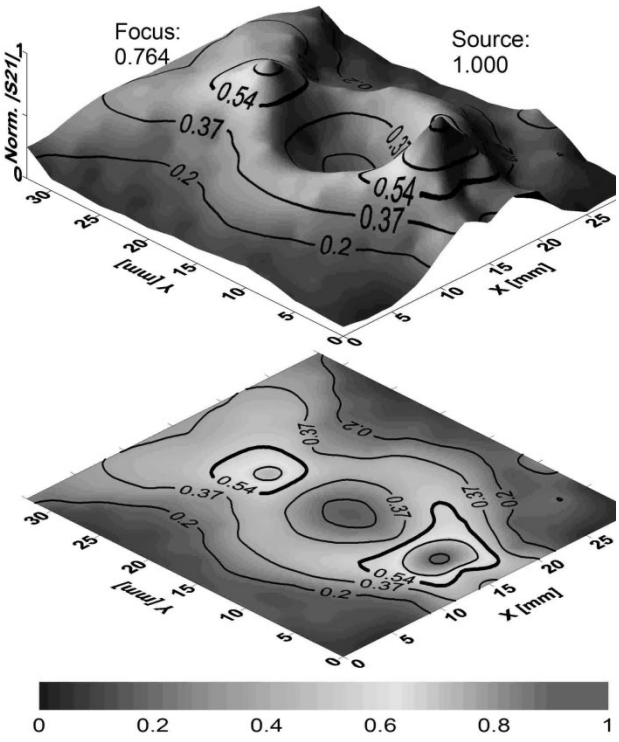

Fig. 12. Focusing measurements at 1.7 GHz showing the normalized S21 magnitude. Heavy contour is at 0.707 of focal maximum of 0.764 (units of normalized $|S21|$).

Returning to the *L-C* grid metamaterial refraction displayed in Fig. 8, we can address the question of how the electromagnetic field and Poynting vector plots would differ, comparing the field calculations carried out at the ground plane level with those carried out at the level of the anisotropic grid. On the ground plane the electric field is necessarily vertical and is plotted in Fig. 13 which also displays the same Poynting vectors as in

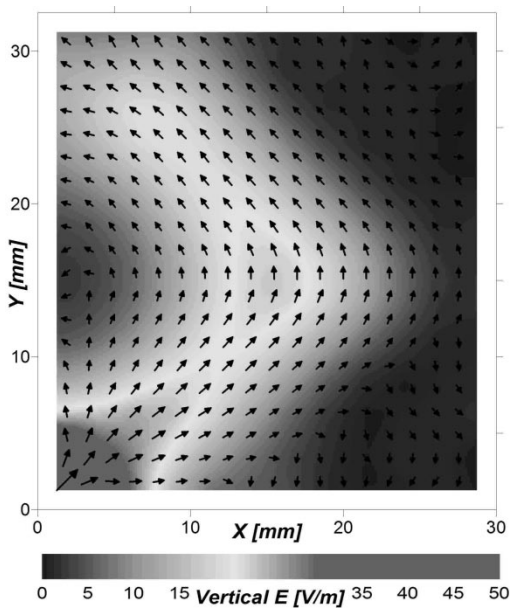

Fig. 13. Simulation results for the fields associated with resonance cone refraction at 1.2 GHz, showing the vertical electric field calculated on the ground plane in the center of each cell. The electric field here is directed entirely out-of-plane while the magnetic field vector lies entirely in the plane.

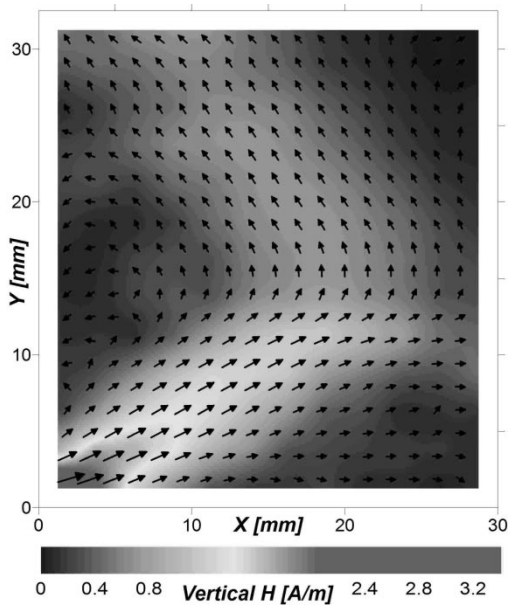

Fig. 14. Simulation results for the fields associated with resonance cone refraction at 1.2 GHz, showing the vertical magnetic field on the grid plane in the center of each cell. The magnetic field here is directed almost entirely out-of-plane while the electric field vector lies almost entirely in the plane.

Fig. 8. As one might expect, the vertical electric field plot is qualitatively similar to the plot of the grid-to-ground voltage in Fig. 8. For comparison, we can plot the simulated normal magnetic field in the plane of the anisotropic grid, along with the corresponding Poynting vector, as shown in Fig. 14. The magnetic field is almost entirely normal to this plane, and its in-plane components as well as the normal component of the electric field are negligible. In the lower left quadrant of the figure, resonance cone formation and outward power flow along the cone are clearly visible. As in Fig. 13, the Poynting flux follows the resonance cone closely, but in Fig. 14, the resonance cone appears at a slightly smaller angle to the x axis compared to the resonance cone on the ground plane. In the upper half of the figure, a negatively refracted resonance cone is visible although weaker than in Fig. 13. Something as yet unexplained is visible in the lower right quadrant of Fig. 14, which is a noticeable Poynting flux directed generally toward the right in the figure. In the same quadrant close to the right edge a small region of elevated magnetic field is seen which extends from the resonance cone in the lower half but does not appear at the angle expected for specular reflection. The resonance cone appears to have split into one part which is refracted and another part which is deflected along the boundary.

IV. Conclusion

The densely-loaded *L*-*C* anisotropic grid over ground has been constructed, tested and then simulated using a moment-method program, displaying good agreement between measurement and simulation. The near fields exhibit in simulation and experiment the expected resonance cone phenomena, namely negative refraction at an interface and focusing from a point source to a small near-field region defined as 3 dB down from the focal peak and fitting within a square measuring no more than 1/25th of a free-space wavelength on a side. Power flow was shown to be parallel to the resonance cones, tracking them closely throughout the process of negative refraction. Refraction at an interface was accompanied by negligible specular reflection from the interface and no noticeable transmission in the direction of the incident resonance cone. Very weak parasitic resonance cones associated with weak power flow were observed, presumably resulting from scattering by the inhomogeneities inherent in the periodic grid structure.

The anisotropic grid concept was motivated in part by the properties of an ionized-gas plasma permeated by a steady magnetic field, but it must be noted that the anisotropic *L*-*C* grid with two regions defined by transposed *L* and *C* cannot be realized physically in the form of a plasma, mainly because this would require the impossible, an abrupt spatial step in steady magnetic field as well as a similar step in electron density, in order to create a refractive interface. Therefore the anisotropic grid over ground can be regarded reasonably as a metamaterial, which is one having properties that cannot be realized with normal materials or in natural media.

Although the material described here was made with "commercial off-the-shelf" $\pm 10\%$ accuracy, lumped-element inductors and capacitors, it should be noted that the simulations included finite-length wire interconnections between the lumped elements as well as a full-electromagnetic theoretical basis, so this paper goes well beyond the seemingly circuit-like conceptual structure displayed in Fig. 3. In fact, we have achieved similar results by replacing the lumped elements with distributed elements consisting of meander-line or straight-wire inductors and parallel-conductor capacitors. This brings to mind a significant constraint arising from the interconnect inductances: they tend to diminish the capacitive influence of the lumped capacitors, as well as increasing the inductance in the orthogonal inductive branches.

Eventual applications might include devices such as instantaneous spectrum analyzers or antenna multiplexers. In spite of the emphasis here on the electromagnetics of the resonance cone phenomena, a circuit theory point of view remains valid as a useful approximation. Because, in circuit theory, all interconnect dimensions are regarded as having zero length and all lumped elements are regarded as being infinitesimal, therefore in the present context of devices based on resonance cone phenomena, it appears that there would be no fundamental limit to size reduction, thus, enabling compact designs limited only by the technologies employed to make miniature capacitors and inductors or their equivalents.

ACKNOWLEDGMENT

The authors wish to thank Prof. G. V. Eleftheriades for stimulating discussions.

REFERENCES

[1] F. V. Bunkin, "On radiation in anisotropic media," *Soviet Phys. JETP*, vol. 5, no. 2, pp. 277–283, Sept. 1957.

[2] H. Kogelnik, "On electromagnetic radiation in magneto-ionic media," *J. Res. Natl. Bureau of Standards-D. Radio Propagation*, vol. 64D, no. 5, pp. 515–523, Sept.-Oct. 1960.

[3] H. H. Kuehl, "Electromagnetic radiation from an electric dipole in a cold anisotropic plasma," *Phys. Fluids*, vol. 5, no. 9, pp. 1095–1103, Sept. 1962.

[4] R. K. Fisher and R. W. Gould, "Resonance cones in the field pattern of a short antenna in an anisotropic plasma," *Phys. Rev. Lett.*, vol. 22, no. 21, pp. 1093–1095, May 1969.

[5] H. G. James, "Electrostatic resonance-cone waves emitted by a dipole in the ionosphere," *IEEE Trans. Antennas Propagat.*, vol. 48, pp. 1340–1348, Sept. 2000.

[6] K. G. Balmain, "The impedance of a short dipole antenna in a magnetoplasma," *IEEE Trans. Antennas Propagat.*, vol. AP-12, pp. 605–617, Sept. 1964.

[7] K. G. Balmain and G. A. Oksiutik, "RF probe admittance in the ionosphere: theory and experiment," in *Plasma Waves in Space and in the Laboratory*: Edinburgh Univ. Press, 1969, vol. 1, pp. 247–261.

[8] K. C. Yeh and C. H. Liu, *Theory of Ionospheric Waves*. New York: Academic, 1972, pp. 193–204.

[9] V. G. Veselago, "The electrodynamics of substances with simultaneously negative values of ε and μ," *Soviet Phys. Uspekhi*, vol. 10, no. 4, pp. 509–514, Jan.-Feb. 1968.

[10] J. B. Pendry, "Negative refraction makes a perfect lens," *Phys. Rev. Lett.*, vol. 85, no. 18, pp. 3966–3969, Oct. 2000.

[11] R. A. Shelby, D. R. Smith, and S. Schultz, "Experimental verification of a negative index of refraction," *Sci.*, vol. 292, no. 5514, pp. 77–79, Apr. 2001.

[12] G. V. Eleftheriades, A. K. Iyer, and P. C. Kremer, "Planar negative refractive index media using periodically L-C loaded transmission lines," *IEEE Trans. Microwave Theory Tech.*, vol. 50, pp. 2702–2712, Dec. 2002.

[13] M. A. Tilston and K. G. Balmain, "A multiradius, reciprocal implementation of the thin-wire moment method," *IEEE Trans. Antennas Propagat.*, vol. 38, pp. 1636–1644, Oct. 1990.

[14] K. G. Balmain, A. A. E. Lüttgen, and P. C. Kremer, "Resonance cone formation, reflection, refraction and focusing in a planar anisotropic metamaterial," *IEEE Antennas Wireless Propagat. Lett.*, vol. 1, pp. 146–149, 2002.

Keith G. Balmain (S'56–M'63–SM'85–F'87–LF'97) received the B.A.Sc. degree in engineering physics from the University of Toronto, Toronto, ON, Canada, in 1957. He received the M.S. and Ph.D. degrees in electrical engineering from the University of Illinois, Urbana, in 1959 and 1963, with theses on printed-circuit dipole antennas and spacecraft-borne dipole antennas in anisotropic plasma.

He was an Assistant Professor of electrical engineering at the University of Illinois until 1966. He then joined what is now The Edward S. Rogers Sr. Department of Electrical and Computer Engineering, University of Toronto, where he is a Professor Emeritus. From 1991 to 2001, he was the Senior Chairholder of the NSERC/Bell Canada/Nortel Industrial Research Chair in Electromagnetics. He chaired the Division of Engineering Science for two and a half years until 1987, after which, for a three-year term, he chaired the University of Toronto's Research Board. Currently he leads the Novel Microwave Technologies Thrust within the University of Toronto's Nortel Institute for Telecommunications. His research has included antennas in plasma, broadband antennas, electromagnetic compatibility, human electrostatic discharge, radio wave scattering from power lines and buildings, Space Shuttle EMC prediction, electrostatic charging and discharging in spacecraft dielectrics, and microwave metamaterials. He coauthored the second edition of *Electromagnetic Waves and Radiating Systems* (Englewood Cliffs, NJ: Prentice-Hall, 1968).

Dr. Balmain is a Life Fellow of the IEEE "for contributions to the understanding of log-periodic antennas and antennas in plasma." He was the co-recipient of the IEEE Antennas and Propagation Society (AP-S) 1970 Best Paper Award, and was a co-recipient of a 1992 NASA Group Achievement Award for an "exceptional engineering assessment of plasma effects from electrical grounding for the Space Station Freedom program." He was a member of AP-S AdCom (1974–77), an Associate Editor of *Radio Science* (1978–1980), chair of the Technical Program Committee for the Quebec City 1980 IEEE AP-S International Symposium, and chair of the Organizing Committee for the Toronto 1999 General Assembly of the International Union of Radio Science (URSI).

Andrea A. E. Lüttgen (A'00) received the Diploma (M.Sc.) degree in physics and the Ph.D degree in geophysics from the University of Cologne, Germany, in 1987 and 1992, respectively.

She was a Research Assistant with the University of Cologne until 1993, working mostly on electromagnetic interaction of tethered satellite systems with the ionospheric plasma. She was awarded the NSERC International Fellowship and came to what is now The Edward S. Rogers Sr. Department of Electrical and Computer Engineering, University of Toronto, Toronto, ON, Canada, in 1993, where she is a Research Fellow. Her research interests include microwave metamaterials, antennas in plasmas, and spacecraft charging and discharging effects.

Dr. Lüttgen is a member of the American Geophysical Union.

Peter C. Kremer joined the Radio Astronomy Group of the University of Toronto, Toronto, ON, Canada, as an Engineering Technologist in 1965 after a career as a Radio Officer in the German Merchant Marine. Currently, he is a senior Engineering Technologist with the Electromagnetics Group, The Edward S. Rogers Sr. Department of Electrical and Computer Engineering, University of Toronto. He worked on the development of low noise receivers including Ruby and Rutile traveling-wave masers. His major projects included digital and analog communication equipment for a long baseline interferometer using the Communication Technology (CTS) satellite, and a dual-band-EHF controlled-beam antenna for frequency-hopped signals. He has been involved with many antenna measurement and design projects, including recent ones using novel, synthesized, artificial dielectrics. He has developed procedures to micromachine silicon structures for a variety of compact, lightweight microwave applications. Also, he has designed and developed a series of instruments to measure electrostatic charge accumulation on conductors embedded in spacecraft dielectrics.